Sea level and global ice volumes from the Last Glacial Maximum to the Holocene

Kurt Lambeck[a,b,1], Hélène Rouby[a,b], Anthony Purcell[a], Yiying Sun[c], and Malcolm Sambridge[a]

[a]Research School of Earth Sciences, The Australian National University, Canberra, ACT 0200, Australia; [b]Laboratoire de Géologie de l'École Normale Supérieure, UMR 8538 du CNRS, 75231 Paris, France; and [c]Department of Earth Sciences, University of Hong Kong, Hong Kong, China

This contribution is part of the special series of Inaugural Articles by members of the National Academy of Sciences elected in 2009.

Contributed by Kurt Lambeck, September 12, 2014 (sent for review July 1, 2014; reviewed by Edouard Bard, Jerry X. Mitrovica, and Peter U. Clark)

The major cause of sea-level change during ice ages is the exchange of water between ice and ocean and the planet's dynamic response to the changing surface load. Inversion of ∼1,000 observations for the past 35,000 y from localities far from former ice margins has provided new constraints on the fluctuation of ice volume in this interval. Key results are: (*i*) a rapid final fall in global sea level of ∼40 m in <2,000 y at the onset of the glacial maximum ∼30,000 y before present (30 ka BP); (*ii*) a slow fall to −134 m from 29 to 21 ka BP with a maximum grounded ice volume of ∼52 × 10^6 km^3 greater than today; (*iii*) after an initial short duration rapid rise and a short interval of near-constant sea level, the main phase of deglaciation occurred from ∼16.5 ka BP to ∼8.2 ka BP at an average rate of rise of 12 m·ka^{-1} punctuated by periods of greater, particularly at 14.5–14.0 ka BP at ≥40 mm·y^{-1} (MWP-1A), and lesser, from 12.5 to 11.5 ka BP (Younger Dryas), rates; (*iv*) no evidence for a global MWP-1B event at ∼11.3 ka BP; and (*v*) a progressive decrease in the rate of rise from 8.2 ka to ∼2.5 ka BP, after which ocean volumes remained nearly constant until the renewed sea-level rise at 100–150 y ago, with no evidence of oscillations exceeding ∼15–20 cm in time intervals ≥200 y from 6 to 0.15 ka BP.

sea level | ice volumes | Last Glacial Maximum | Holocene

The understanding of the change in ocean volume during glacial cycles is pertinent to several areas of earth science: for estimating the volume of ice and its geographic distribution through time (1); for calibrating isotopic proxy indicators of ocean volume change (2, 3); for estimating vertical rates of land movement from geological data (4); for examining the response of reef development to changing sea level (5); and for reconstructing paleo topographies to test models of human and other migrations (6). Estimates of variations in global sea level come from direct observational evidence of past sea levels relative to present and less directly from temporal variations in the oxygen isotopic signal of ocean sediments (7). Both yield model-dependent estimates. The first requires assumptions about processes that govern how past sea levels are recorded in the coastal geology or geomorphology as well as about the tectonic, isostatic, and oceanographic contributions to sea level change. The second requires assumptions about the source of the isotopic or chemical signatures of marine sediments and about the relative importance of growth or decay of the ice sheets, of changes in ocean and atmospheric temperatures, or from local or regional factors that control the extent and time scales of mixing within ocean basins.

Both approaches are important and complementary. The direct observational evidence is restricted to time intervals or climatic and tectonic settings that favor preservation of the records through otherwise successive overprinting events. As a result, the records become increasingly fragmentary backward in time. The isotopic evidence, in contrast, being recorded in deep-water carbonate marine sediments, extends further back in time and often yields near-continuous records of high but imprecise temporal resolution (8). However, they are also subject to greater uncertainty because of the isotope signal's dependence on other factors. Comparisons for the Holocene for which the direct measures of past sea level are relatively abundant, for example, exhibit differences both in phase and in noise characteristics between the two data [compare, for example, the Holocene parts of oxygen isotope records from the Pacific (9) and from two Red Sea cores (10)].

Past sea level is measured with respect to its present position and contains information on both land movement and changes in ocean volume. During glacial cycles of ∼10^5 y, the most important contribution with a global signature is the exchange of mass between the ice sheets and oceans, with tectonic vertical land movements being important mainly on local and regional scales. Global changes associated with mantle convection and surface processes are comparatively small on these time scales but become important in longer, e.g., Pliocene-scale, periods (11). Changes in ocean volume associated with changing ocean temperatures during a glacial period are also small (12).

The sea-level signal from the glacial cycle exhibits significant spatial variability from its globally averaged value because of the combined deformation and gravitational response of the Earth and ocean to the changing ice-water load. During ice-sheet decay, the crust rebounds beneath the ice sheets and subsides beneath the melt-water loaded ocean basins; the gravitational potential and ocean surface are modified by the deformation and changing surface load; and the planet's inertia tensor and rotation changes, further modifying equipotential surfaces. Together, this response of the earth-ocean system to glacial cycles is referred to as the glacial isostatic adjustment (GIA) (13–17). The pattern of the spatial variability is a function of the Earth's rheology and of the glacial history, both of which are only partly known. In particular, past ice thickness is rarely observed and

Significance

Several areas of earth science require knowledge of the fluctuations in sea level and ice volume through glacial cycles. These include understanding past ice sheets and providing boundary conditions for paleoclimate models, calibrating marine-sediment isotopic records, and providing the background signal for evaluating anthropogenic contributions to sea level. From ∼1,000 observations of sea level, allowing for isostatic and tectonic contributions, we have quantified the rise and fall in global ocean and ice volumes for the past 35,000 years. Of particular note is that during the ∼6,000 y up to the start of the recent rise ∼100–150 y ago, there is no evidence for global oscillations in sea level on time scales exceeding ∼200 y duration or 15–20 cm amplitude.

Author contributions: K.L. designed research; K.L., H.R., A.P., Y.S., and M.S. performed research; Y.S. contributed field data; K.L., H.R., A.P., Y.S., and M.S. analyzed data; K.L. and H.R. wrote the paper; and A.P. and M.S. developed software.

Reviewers: E.B., CEREGE; J.X.M., Harvard University; and P.U.C., Oregon State University.

The authors declare no conflict of interest.

Freely available online through the PNAS open access option.

[1]To whom correspondence should be addressed. Email: kurt.lambeck@anu.edu.au.

This article contains supporting information online at www.pnas.org/lookup/suppl/doi:10.1073/pnas.1411762111/-/DCSupplemental.

questions remain about the timing and extent of the former ice sheets on the continental shelves. The sea-level response within, or close to, the former ice margins (near-field) is primarily a function of the underlying rheology and ice thickness while, far from the former ice margins (far-field), it is mainly a function of earth rheology and the change in total ice volume through time. By an iterative analysis of observational evidence of the past sea levels, it becomes possible to improve the understanding of the past ice history as well as the Earth's mantle response to forces on a 10^4 y to 10^5 y time scale.

In this paper, we address one part of the Earth's response to the glacial cycle: the analysis of far-field evidence of sea-level change to estimate the variation in ice and ocean volumes from the lead into the Last Glacial Maximum (LGM) at ~35,000 y ago (35 ka BP) to the start of the instrumental records. Such analyses can either be of high-resolution records of a single data type from a single location or of different sea-level indicators from many different locations. We have adopted the latter approach. Most sea-level indicators provide only lower (e.g., fossil coral) or upper (e.g., fossil terrestrial plants) limiting values, and multiple data-type analyses of both upper and lower limiting measurements are less likely to be biased toward one or the other limit. Tectonic displacement of the crust is always a potential contaminator of the sought signal, and a multiplicity of data from tectonically "stable" regions is more likely to average out any undetected tectonic effects as well as any uncertainties in the above-mentioned GIA contributions.

Analysis Strategy

In a zero-order approximation, the change in sea level during glacial cycles is the ice-volume equivalent sea level (esl) $\Delta\zeta_{esl}$ defined as

$$\Delta\zeta_{esl}(t) = -\frac{1}{\rho_o}\int_t \frac{1}{A_o(t)}\frac{d\Delta M_{ice}}{dt}dt \qquad [1]$$

where ΔM_{ice} is the change in ice mass on the continents and grounded on the shelves at time t with respect to present, A_o is the ocean area defined by the coastline and ice grounding line at t, and ρ_o is the average density of the ocean. Superimposed on this is the response of the earth and ocean surface to the changes in loading. Hence, as a first approximation, the relative sea-level $\Delta\zeta_{rsl}$ at a location ϕ and time t is

$$\Delta\zeta_{rsl}(\phi,t) = \Delta\zeta_{esl}(t) + \delta\zeta^{iso}_{ice}(\phi,t) + \delta\zeta^{iso}_{water}(\phi,t) \qquad [2]$$

where $\delta\zeta^{iso}_{ice}(\phi,t)$ and $\delta\zeta^{iso}_{water}(\phi,t)$ are the isostatic contributions from the changing ice and water loads, respectively. Because of the direct gravitational attraction of the ice sheets and deformation of the ocean basin during the glacial cycle, $\delta\zeta^{iso}_{water}(\phi,t)$ is not independent of ice sheet geometry. Consequently, higher-order iterative solutions are necessary to solve [**2**].

In the absence of tectonics, the dominant departure of far-field sea level from its global mean [**1**] is due to $\delta\zeta^{iso}_{water}(\phi,t)$ and results in a strong spatial variability of $\Delta\zeta_{rsl}(\phi,t)$ across continental margins and within partially enclosed ocean basins that is dependent on mantle rheology, the amount of water added into the oceans, and the rate at which it is discharged, but is relatively insensitive to where this melt water originated. Typically, during the melting phase, $\delta\zeta^{iso}_{water}(\phi,t)$ is about 15–25% of $\Delta\zeta_{esl}(t)$ and leads to near-coastal observations of LGM sea level being systematically less than the corresponding $\Delta\zeta_{esl}(t)$. When deglaciation ceases, the seafloor continues to deform because of the viscous nature of the mantle, and sea levels particularly at continental edges fall slowly until all load stresses have relaxed. This mechanism often produces small highstands at ~5–7 ka BP that mark the end of the dominant melting period (15, 16, 18).

The $\delta\zeta^{iso}_{ice}(\phi,t)$ reflects mantle-scale flow induced by the changes in ice load. This signal includes the evolution of a broad trough and bulge system that extends several thousand kilometers beyond the ice margin, as a combined result of surface deformation and gravitational potential change (the "geoidal" bulge). Beyond these features, $\delta\zeta^{iso}_{ice}(\phi,t)$ shows less spatial variability than $\delta\zeta^{iso}_{water}(\phi,t)$ and is relatively insensitive to the details of the ice load, but the amplitudes of these signals are not negligible and are earth-rheology dependent.

The challenge is, in the presence of imperfect and incomplete data, to invert the complete formulation of [**2**] for both the earth and ice unknowns. This challenge is approached here through the following iterative procedure: (*i*) Start with far-field sea-level data, assume $\Delta\zeta_{rsl} = \Delta\zeta_{esl}$ and using [**1**] estimate a first approximation of ice mass or volume function $\Delta V_{ice}(t)$. (*ii*) Distribute this ice between the known ice sheets, guided by either published information or by glaciological hypotheses and with ice advance and retreat histories, depending on the state of knowledge of the particular ice sheet. (*iii*) Invert far-field sea-level data for earth rheology parameters E (mantle viscosity, elastic thickness of the lithosphere) and for a corrective term $\delta\zeta_{esl}$ to the nominal $\Delta\zeta^0_{esl}$ corresponding to step *ii*, yielding an improved approximation of ice volume function $\Delta V_{ice}(t)$. (*iv*) Analyze sea-level data separately for each of the major ice sheets (near-field analyses) and, starting with the ice models from step *ii*, invert for both E and corrections to ice-thickness functions I. (*v*) Impose the condition that the sum of the individual ice volume functions equals $\Delta V_{ice}(t)$ from step *iii* and distribute any discrepancies between the ice sheets. (*vi*) Repeat steps *iii*–*v* until convergence has been achieved.

Advantages of this approach include the ability to analyze individual ice sheets with different resolutions depending on the state of a priori knowledge of the ice sheet and quality of the observational data, as well as to make a first-order estimate for lateral variation in mantle viscosity.

Observational Evidence

The principal sources for quantitative sea-level information are from sediment and coral records whose depositional environments relative to mean sea level (MSL) are assumed known and whose ages have been determined either by radiocarbon or uranium-series dating. In the former case, all ^{14}C ages have been calibrated using either the calibrations provided by the original authors or the IntCal09 calibration (19). Reservoir and isotopic fractionation corrections have been applied where appropriate.

Corals provide lower-limit estimates of mean-low-water-spring (MLWS) tide, but their growth depth range $\delta\zeta_d$ is species and environment dependent (20). Assuming that the modern range is representative of the past growth range, the adopted mean sea level from in situ fossil corals of age t at elevation ζ (all vertical measures are positive upward) is

$$\Delta\zeta_{rsl}(\phi,t) = \zeta(\phi,t) - \delta\zeta_d/2 - \delta\zeta_{tide}$$

where $\delta\zeta_{tide}$ is the MLWS level with respect to MSL (with the further assumption that, in the absence of paleo tide amplitude information, there has been no significant change in tides). The adopted precision estimate of the observation is $\Delta\zeta_d/2$, added in quadrature to other error sources. Greater uncertainties can arise at times of very rapid sea-level rise if reef formation cannot keep up. In some special morphological forms, the in situ coral can be related more directly to MLWS, as is the case of microatolls where the coral grows up to this limiting level before growing radially outward at the MLWS level (21). Observed records are restricted to the past ~6–7 ka, when far-field sea-level change was slow enough for the microatoll development to be able to keep up with change (22). The most complete record is from Kiritimati Atoll (23). The principal coral records for the late glacial period are from Barbados (24–26), Tahiti (27, 28), Huon

Peninsula of Papua New Guinea (29, 30), the western Indian Ocean (31), and the Great Barrier Reef of Australia, supplemented for the past 7 ka with other observations from the Australian region and the Indian Ocean (Fig. 1 and *SI Appendix*, Table S1).

The sedimentological evidence consists of age–depth relationships of material formed within a known part of the tidal range, such as terrestrial plants representative of the highest tidal zone or microfaunal material representative of a lower tidal range (32) (observations that provide only limiting estimates have been excluded). This evidence has the ability to provide high-precision results if restricted to materials with well-understood depositional ranges, but they also present their own difficulties. Is the dated material within the sediment layer in situ? Has there been age contamination by transport of older carbon into the sediment sequence? Has compaction of the sediment column subsequent to deposition been important? Significant data sources included are from the Sunda Shelf (33, 34), the Indian Ocean (35, 36), the Bonaparte Gulf (37, 38), New Zealand (39), Singapore (40, 41), Malaysia (42), and from the South China Sea to the Bohai Sea. Many of the Asian observations are from large delta systems, and comparisons of such data with observations from adjacent sites often indicate lower levels of the former, corresponding to differential subsidence rates of the order of 1 mm·y^{-1} for the past ~8 ka. Hence data from the deltas of Chao Phraya of Thailand, Mekong and Red rivers of northern Vietnam, and Pearl and Yangtze rivers of China, have not been used for the purpose of estimating the esl function.

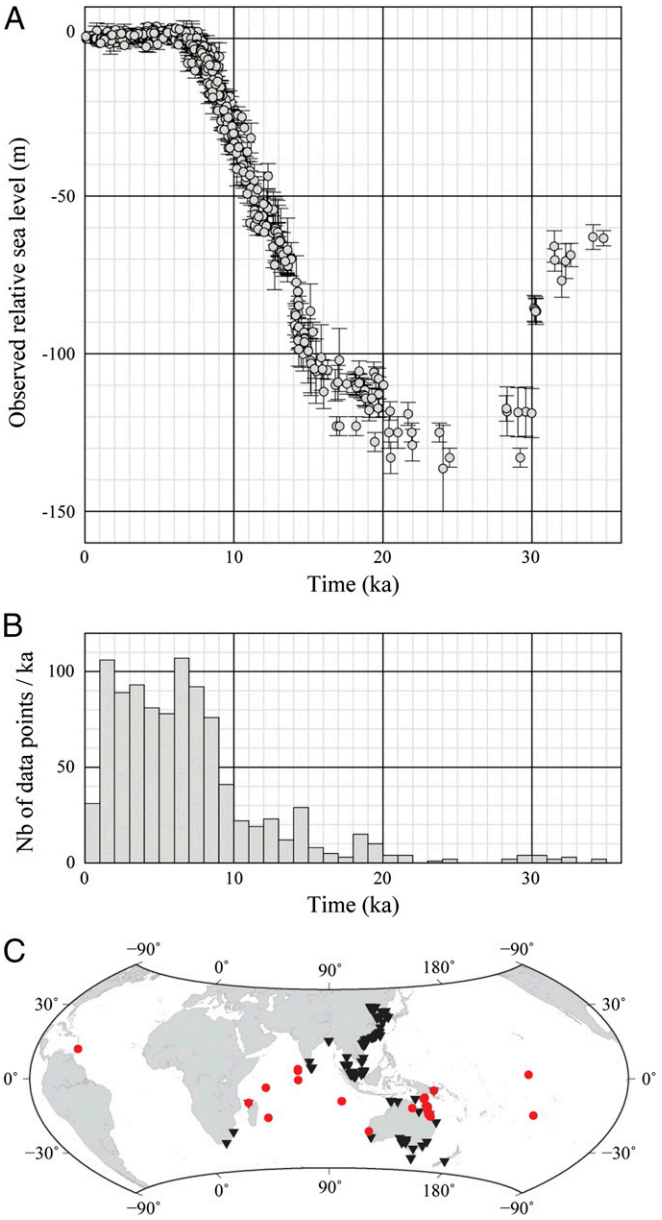

Fig. 1. Distribution of far-field sea-level data for the past 35 ka. (*A*) Depth–age relationship of all data with 2σ error estimates. (*B*) Time distribution of the data. (*C*) Geographic distribution of all far-field coral (red dot) and sediment (black triangles) data.

Where possible, the selected data are from tectonically stable regions: away from plate margins and marked by an absence of seismic activity and recent faulting. Where available, evidence for the Last Interglacial (marine isotope stage 5.5) shoreline, formed when, globally, sea levels were ~4–8 m above present (43, 44), has been used to assess the long-term stability of the region or to correct for tectonic displacement. Both Huon Peninsula and Barbados have been subject to uplift, and Tahiti to subsidence (*SI Appendix*, Text S1). The eastern Asian margin in many locations is characterized by rifting of Cenozoic age and postrift thermal subsidence (45), but the expected rates are small on time scales of the past 20 ka compared with the GIA signals and observational uncertainties, and no corrections have been applied.

Inversion Results: Mantle Rheology

The observation equation is

$$\Delta\zeta_{obs}(\phi,t)+\varepsilon_{obs}=\Delta\zeta_{predicted}(\phi,t)$$
$$=\Delta\zeta^{0}_{esl}(t)+\delta\zeta_{esl}(t)+\delta\zeta^{iso}_{ice}(\phi,t)+\delta\zeta^{iso}_{water}(\phi,t) \quad [3]$$

where ε_{obs} are corrections to the observations of relative sea level and $\delta\zeta_{esl}(t)$ is a corrective term to $\Delta\zeta^{0}_{esl}(t)$, parameterized in the first instance as mean values in time bins of 1,000 y from present to 22 ka BP, with larger bins for the data-sparse intervals 22–26 ka BP, 26–31 ka BP, and 31–36 ka BP (Fig. 1). The inversion for the earth-model parameters E and $\delta\zeta_{esl}(t)$ is by forward modeling through E space in which for any E_k ($k = 1..K$), the corresponding $\delta\zeta_{k,esl}(t)$ is estimated by weighted least squares. The minimum value of the variance function Ψ^2_k in E space,

$$\Psi^2_k=\frac{1}{M}\sum_{m=1}^{M}\left\{\left[\Delta\zeta^{m}_{obs}-\left(\Delta\zeta^{0}_{esl}+\delta\zeta_{k,esl}+\delta\zeta_{k,iso}\right)\right]/\sigma^{m}\right\}^2, \quad [4]$$

is then sought, where $\delta\zeta_{k,iso}$ is the total isostatic correction for E_k and σ^m is the SD of the mth observation ($m = 1..M$). The E space is initially restricted to a three-layered model of the mantle: elastic lithosphere (including the crust) defined by an effective elastic thickness H, upper mantle from the base of the lithosphere to the 670 km seismic discontinuity with a depth-averaged effective viscosity η_{um}, and a lower mantle viscosity extending down to the core-mantle boundary of depth-averaged effective viscosity η_{lm}. Elastic moduli and density are based on realistic depth profiles determined from seismic data inversions. These approximate models nevertheless describe well the response of the Earth to surface loading at periods and mantle-lithosphere stress levels of glacial cycles (46, 47). The E search is conducted within the confines

$$\begin{aligned}&\text{Effective lithospheric thickness:} && 30\le H_1\le 140 \text{ km.}\\ &\text{Effective upper-mantle viscosity:} && 10^{19}\le\eta_{\rm um}\le 10^{21} \text{ Pa s.}\\ &\text{Effective lower-mantle viscosity:} && 5\times10^{20}\le\eta_{\rm lm}\le 10^{24} \text{ Pa s.}\end{aligned} \quad [5]$$

that span parameters found in earlier far- and near-field analyses. The theory for the viscoelastic solution of earth deformation is

based on the transformation of the elastic formulation into the Laplace domain using the correspondence principle and then inverting the Laplace-domain solution back into the time domain (13, 15, 48). This latter inversion is carried out using a pure collocation method (49) that has the potential to become unstable when the ratio of the relaxation times of the two mantle layers becomes very large, and, for numerical reasons, the above E space is restricted to models for which $\eta_{lm}/\eta_{um} \leq 500$ (see *Discussion and Conclusions*).

In the first iteration solution, a conservative data-quality criterion $\left|(\Delta\zeta_{obs} - \Delta\zeta_{predicted})/\sigma_{obs}\right| > 6$ has been adopted to examine gross discrepancies without rejecting observations that may point to rapid changes in ice volumes not captured by the parameterized $\delta\zeta_{esl}(t)$ function. Only where such large discrepancies are incompatible with other observations close in location and time are they excluded, and 18 observations, of a total of 992, have been rejected. The Barbados record was not used in early iterations because it is from the outer edge of the geoidal bulge around the North American ice sheet and sea-level response there may be more sensitive to $\delta\zeta^{iso}_{ice}(\phi, t)$ than sites further from the ice margin, as well as to potential differences in mantle viscosity beneath continents and oceans and local mantle structure associated with the descending lithospheric slab (50). However, tests with and without this data yielded near-identical results for both E and $\delta\zeta_{esl}(t)$, and, in all subsequent iterations, observations from Barbados (but not from other Caribbean sites closer to the former ice margin) have been included.

The resulting variance function Ψ^2_k is illustrated in Fig. 2. The minimum value of ~2.8 exceeds the expected value of unity. About 10% of the observations contribute nearly 50% to this variance, but excluding this information from the analysis does not lead to different E. That $\Psi^2_k > 1$ indicates either an underestimation of the observational uncertainties or unmodeled contributions to sea level. Of the former, conservative estimates of observational accuracies have already been made, but, in some instances, local tectonic or subsidence contributions, or corrections for the coral growth range, may be more important than assumed. Part of the latter may be a consequence of rapid changes in ice volume not well captured by the adopted bin sizes, but solutions with smaller bins give identical results for E. Part may be a consequence of the oversimplification of the depth dependence of the viscosity layering, but solutions with further viscosity layering in the upper mantle do not lead to a variance reduction, and two layered upper-mantle models with their boundary at the ~400-km seismic discontinuity lead to a minimum variance solution for near-zero viscosity contrast across this boundary. A further possible contributing factor is the assumption of lateral uniformity of viscosity in the mantle. Separate solutions for continental-margin and midocean-island data do not require lateral variation, partly because the island data are limited in their distribution and partly because the resolution of island data for depth dependence of viscosity is intrinsically poor. Solutions excluding the eastern margin of Asia also lead to the same E. Hence the resulting E parameters are descriptive of the mantle response for continental margins and midocean environments across the Indian and eastern Pacific Oceans and the margins of Australia, East Africa, and southern and eastern Asia.

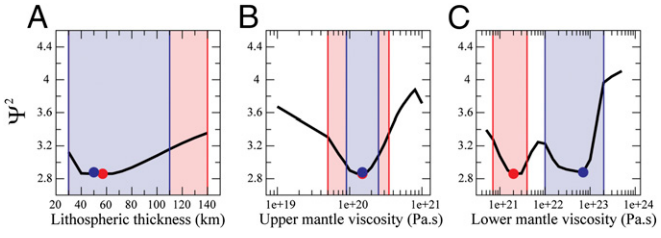

Fig. 2. Minimum variance function Ψ^2_k [4] as function of (*A*) lithospheric thickness H, (*B*) upper-mantle viscosity η_{um}, and (*C*) lower-mantle viscosity η_{lm} across E space defined by [5] with $\eta_{lm}/\eta_{um} \leq 500$. Unique solutions are found for H and η_{um} but two minima are identified for η_{lm}: a low lower-mantle viscosity solution at η_{lm} ~2×10^{21} Pa s (red dot) and a high lower-mantle viscosity solution at η_{lm} ~10^{23} Pa s (blue dot). The corresponding 95% confidence limits Φ^2_k [6] are defined by the red and blue bands.

Confidence limits for the E across the space [5] are estimated using the statistic

$$\Phi^2_k = \frac{1}{M}\sum_{m=1}^{M}\left\{\left(\Delta\zeta^m_{k,predicted} - \Delta\zeta^m_{k^*,predicted}\right)\Big/\sigma^m\right\}^2 \qquad [6]$$

where $\Delta\zeta^m_{k^*,predicted}$ are the predicted relative sea levels for observation m and earth model E_{k^*} that correspond to the least variance solution [4]. If observational variances are appropriate and the model is correct and complete, the contour $\Phi^2_k = 1.0$ defines the 67% confidence limits of the minimum variance solution. Of the E_k, η_{um} is well constrained (Fig. 2), with the preferred minimum variance occurring at 1.5×10^{20} Pa s [with 95% confidence limits of ~$(1, 2) \times 10^{20}$ Pa s]. Resolution for lithospheric thickness is less satisfactory and, while the solutions point to a minimum Ψ^2_k at between 40 km and 70 km, the $\Phi^2_k \leq 1$ criterion indicates only that very thick lithospheres can be excluded. This lack of resolution is because (*i*) midocean small-island data have little resolution for H and (*ii*) the distribution of the observations from near the present continent-ocean boundary is insufficient to fully reflect the gradients in $\Delta\zeta_{rsl}(t)$ predicted across this boundary. The solution for η_{lm} is least satisfactory of all (Fig. 2*C*) and points to two local minima, a "low" viscosity solution at 2×10^{21} ($7 \times 10^{20} - 4 \times 10^{21}$) Pa s and a "high" viscosity solution of ~7×10^{22} ($1 \times 10^{22} - 2 \times 10^{23}$) Pa s: An addition of a uniform layer of melt water, whose spatial characteristics are dominated by ocean-basin-scale wavelengths, predominantly stresses the lower mantle. Thus, the question remains whether the geographic variability of the data set is adequate for a complete separation of E and $\Delta\zeta_{esl}(t)$ or whether a unique separation of ice and earth parameters is even possible. We keep both solutions for the present and examine their implications on the ice volume estimates below.

The $\delta\zeta_{esl}(t)$ for the two solutions (Fig. 3) implies that the global estimate of ice volume needs a correction of ~5–10% for some epochs, but the far-field analysis alone does not allow this change to be attributed to one ice sheet or another. To evaluate the possible dependence of the estimates of both E and $\Delta\zeta_{esl}(t)$ on how $\delta\zeta_{esl}(t)$ is distributed, we have considered three options in which: (*i*) the $\delta\zeta_{esl}(t)$ for the LGM and late-glacial period is attributed to the North American ice sheet, (*ii*) the same as option *i* but with the Holocene $\delta\zeta_{esl}(t)$ attributed to Antarctica, and (*iii*) with $\delta\zeta_{esl}(t)$ attributed to Antarctica for the entire interval. The solution for E and a further corrective term to $\Delta\zeta_{esl}$ is then repeated for each of these so-modified ice sheets. This results in equivalent results for E and to a rapid convergence for the $\Delta\zeta_{esl}$ function (*SI Appendix*, Table S2), justifying thereby the basic assumption that the far-field analysis is not critically dependent on the distribution of the ice between the component ice sheets.

Inversion Results: Ice-Volume Equivalent Sea Level

The above parameterization of $\delta\zeta_{esl}(t)$ (Fig. 3) results in a low temporal resolution of $\delta\zeta_{esl}(t)$ that could preclude detection of changes in sea level in intervals <1,000 y. Thus, once optimum effective earth parameters are established that are independent of the details of the ice model, we adopt a post E solution

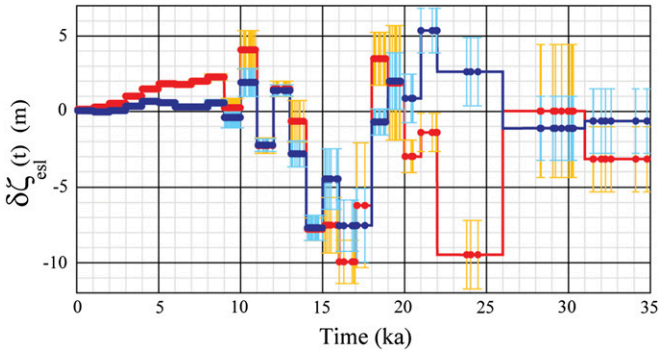

Fig. 3. Low-definition solutions (1,000-y time bins) for the corrective term $\delta\zeta_{esl}(t)$ for the two lower-mantle viscosity solutions (low-viscosity solution in red with yellow error bars and high-viscosity solution in blue with pale blue error bars).

processing approach to solve for the incremental $\delta\zeta_{esl}(t)$ in which each observation $\Delta\zeta^m_{obs}(\phi,t)$ provides an estimate of esl

$$\Delta\zeta^m_{esl}(t) = \Delta\zeta^m_{obs}(\phi,t) - \left[\Delta\zeta^m_{k^*,predicted}(\phi,t) - \Delta\zeta^0_{esl}(t)\right] \qquad [7a]$$

with

$$\left(\sigma^m_{esl}\right)^2 = \left(\sigma^m_{obs}(\phi,t)\right)^2 + \left(\sigma^m_{k^*,predicted}(t)\right)^2. \qquad [7b]$$

The variance $\left(\sigma^m_{k^*predicted}(t)\right)^2$ follows from the variance of the predicted values across the E space defined by the $\Phi^2_k \le 1$ according to

$$\left(\sigma^m_{k^*,predicted}\right)^2 = \left[\sum_k \left(\Delta\zeta^m_{k^*,predicted} - \Delta\zeta^m_{k,predicted}\right)^2 \Big/ \sigma^2_k\right] \Big/ \sum_k 1/\sigma^2_k \qquad [8]$$

with

$$\sigma^2_k = \left[\left(1-\Phi^2_k\right)\right]^2.$$

The underlying signal in the resulting noisy time series is then estimated using the transdimensional Markov chain Monte Carlo approach (51) that allows abrupt or rapid changes to be quantified against a background of long-term trends and that infers the probability distributions on the number and location of change points, as well as the trends between change points. This produces an ensemble of candidate time series curves, the collective density of which follows a Bayesian a posteriori probability density function (PDF) defined by the product of a likelihood and a priori PDF on control parameters. The algorithm avoids the need to impose artificial constraints on model complexity by using a flexible parameterization of the time series with a variable number of unknowns but at the same time remains parsimonious in that it eliminates unwarranted detail in the reconstructed signal. The mean of the ensemble is taken as an objective estimate of the underlying "denoised" time series while uncertainty estimates are obtained through appropriate projections of the ensemble. Uncertainty estimates, in terms of probability density functions, are obtained for the entire time signal as well as location of the change points representing abrupt changes in gradient (*SI Appendix*, Text S2 and Fig. S1).

Fig. 4 illustrates the result corresponding to the high-viscosity lower mantle model, and that for the low-viscosity lower mantle is given in *SI Appendix*, Fig. S2. Solution with and without the China data yield indistinguishable results, and the introduction of this generally lower-quality material has not distorted the inferences that can be drawn about rates of global sea-level change but, rather, reinforces them.

Discussion and Conclusions

On time scales of 10^5 years and less, sea-level change at tectonically stable regions is primarily a function of changing ice volumes and the Earth's response to the changing ice-water load, but neither the ice history nor the response function is independently known with the requisite precision for developing predictive models. Observations of sea level through time do provide constraints on the ice and rheology functions, but a complete separation of the two groups of parameters has not yet been achieved. Separation of the analysis into far-field and near-field areas provides some resolution, but ambiguities remain: a consequence of inadequate a priori information on ice margin evolution and ice thickness, observational data that deteriorates in distribution and accuracy back in time, the likelihood of lateral variations in the planet's rheological response, and the ever-present possibility of tectonic contributions.

We have focused here on the far-field analysis of nearly 1,000 observations of relative sea level for the past 35 ka, underpinned by independent near-field analyses for the individual major ice sheets of the Northern Hemisphere and inferences about the past Antarctic ice sheet. Within the confines of model assumptions and with one caveat, a separation can be achieved of effective rheology parameters for the mantle beneath the oceans and continental margins and the change in total ice volume or ice-volume esl. The caveat is that two solutions are possible, characterized as high-viscosity and low-viscosity lower-mantle models, each with its own esl function (*SI Appendix*, Fig. S2). One approach to separate earth and ice parameters could be to search for "dip-stick" sites (52) where the glacioisostatic and hydroisostatic components cancel and $\Delta\zeta_{rsl}(\phi,t) = \Delta\zeta_{esl}(\phi,t)$. However, such contours do exhibit time and E dependence, and there are few observations that actually lie close to the $\Delta\zeta_{iso} = 0$ contour at any epoch (*SI Appendix*, Fig. S3).

The esl obtained for the two solutions (Fig. 4 and *SI Appendix*, Fig. S2) differ in two important respects: (*i*) at the LGM, the low-viscosity model requires ~2.7×10^6 km^3 (~7 m esl) more ice at the maximum glaciation than the high-viscosity model, and (*ii*) during the mid to late Holocene (the past ~7 ka), the low-viscosity model requires less ice (~0.5×10^6 km^3 or ~1.3 m esl at 6 ka BP) than the high-viscosity model (the relaxation in the low-viscosity model is more complete than for a high-viscosity model). Of these, the first difference may provide some guide to the choice of solution.

The changes in Antarctic ice volume since the LGM remain poorly known, and published estimates differ greatly: ~25–35 m of esl from the difference in far-field and Northern Hemisphere near-field estimates of changes in ice volume (53), ~20 m from the combination of such methods with the inversion of rebound data from the Antarctic margin (54), ~10–18 m from glaciological models (55, 56), and ~10 m from combined glaciological and geological modeling (57). In developing our component ice sheets, we have used an iterative approach in which, at any step, the Antarctic ice-volume function is the difference between the far-field derived global estimate and the sum of the Northern Hemisphere and mountain glacier ice volumes for that iteration. This "missing" ice is then distributed within the ice sheet to respect the LGM Antarctic margin (58) and with the assumption that ice elevation profiles across the shelf and into the interior approximate a quasi-parabolic form (59). Thus, the intent of this ice sheet is only to preserve the global ocean–ice mass balance and not to produce a realistic rebound model for far-southern latitudes. The starting iteration of the present far-field solution has an Antarctic contribution to esl of 28 m (equivalent to ~10^7 km^3 of ice, with a large fraction of this ice grounded on the shelves; see Eq. **1**). For the high-viscosity solution this is reduced to ~23 m

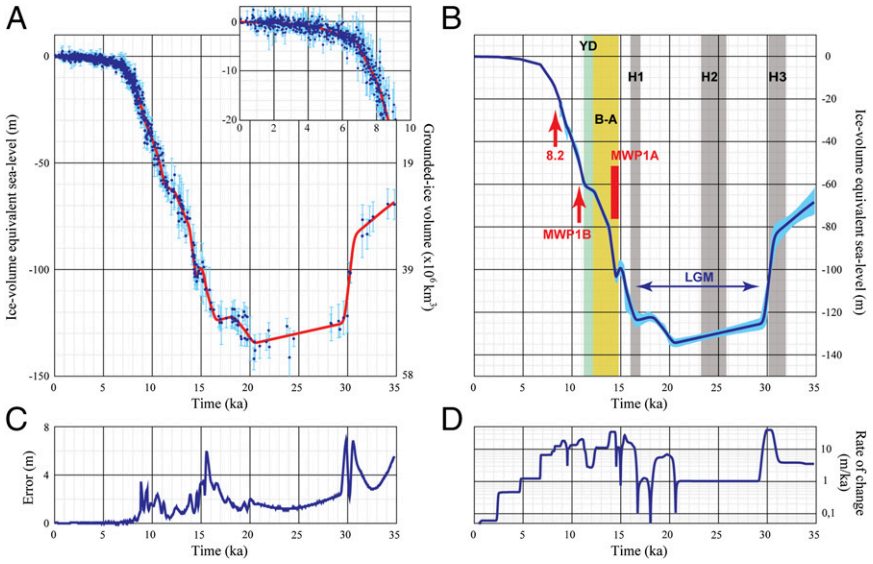

Fig. 4. Solution for the ice-volume esl function and change in ice volume. (*A*) Individual esl estimates (blue) and the objective estimate of the denoised time series (red line). The *Inset* gives an expanded scale for the last 9,000 y. (*B*) The same esl estimate and its 95% probability limiting values. Also shown are the major climate events in the interval [the Last Glacial Maximum (LGM), Heinrich events H1 to H3, the Bølling-Allerød warm period (B-A), and the Younger Dryas cold period (Y-D)] as well as the timing of MWP-1A, 1B, and the 8.2 ka BP cooling event. (*C*) The 95% probability estimates of the esl estimates. (*D*) Estimates of sea-level rate of change.

whereas it is increased to ∼30 m for the low-viscosity solution. The choice of model could then be made on the basis of how much ice can plausibly be stored in Antarctica during the LGM, consistent with other geological and glaciological constraints. On the basis of the comparison with independent estimates (55–57), we favor the high-viscosity model.

Both solutions point to an ongoing slow increase in ocean volume after 7 ka BP, even though melting of the large Northern Hemisphere ice sheets had largely ceased by this time. The high northern latitude Holocene Climate Optimum peaked between 6 and 4 ka BP, and some Greenland ice-margin retreat occurred at least locally (60, 61). There is also evidence that some Antarctic melting occurred after ∼6 ka BP (62). Furthermore, high and midlatitude mountain glaciers, including remnants of Late Pleistocene arctic and subarctic ice caps, may also have continued to decrease in volume (63). However, in all cases, there is not enough observational evidence to independently constrain global estimates of ice-mass fluctuations during this post-7-ka period to permit discrimination between the two esl solutions.

One option is to impose constraints on the lower-mantle viscosity from sources independent of the far-field results. Our analyses of rebound data from formerly glaciated regions (64) and of deglaciation-induced changes in the dynamic flattening and rotation of the Earth (65–67) are consistent with the high-viscosity results, although these solutions are also ice-model dependent. Inversions of geoid and seismic tomographic data are less sensitive to the choice of ice models (the observed geoid needs corrections for the GIA contribution) and point to an increase in depth-averaged mantle viscosity of one to three orders of magnitude from average upper to lower mantle (68–73). Likewise, inferences of viscosity from the sinking speed of subducted lithosphere also point to high (3–5) × 10^{22} Pa s values for the lower-mantle viscosity (74). On this basis, and because it yields the smaller volume for the LGM Antarctic ice volume, we adopt the high-viscosity lower-mantle solution.

The adopted esl function illustrated in Fig. 4 and *SI Appendix*, Table S3, shows many features previously identified in one or more individual records but which, because it is based on geographically well-spaced observations corrected for the isostatic contributions, will reflect more accurately the changes in globally averaged sea level and ice volume. These features are:

i) A period of a relatively slow fall in sea level from 35 to 31 ka BP followed by a rapid fall during 31–29 ka. This is based on data from Barbados, Bonaparte Gulf, Huon Peninsula (Papua New Guinea), and a few isolated observations from the Malay Peninsula and the Bengal Fan. It points to a period of rapid ice growth of ∼25 m esl within ∼1,000 y to mark the onset of the peak glaciation, consistent with the transition out of the Scandinavian Ålesund Interstadial into the glacial maximum (75), although this ice sheet alone is inadequate to contribute 25 m to esl. Chronologically, the timing of the rapid fall corresponds to the nominal age for the Heinrich H3 event (76, 77).

ii) Approximately constant or slowly increasing ice volumes from ∼29–21 ka BP. The data for this interval are sparse but are from geographically well-distributed sites (Barbados, Bonaparte, Bengal Fan, East China Sea, and Maldives). The slow increase in ice volume is consistent with eastward and southward expansion of the Scandinavian ice sheet during the LGM (78) as well as with the southward advance of the Laurentide ice sheet (79). The esl reaches its lowest value of ∼134 m at the end of this interval, corresponding to ∼52 × 10^6 km^3 more grounded ice—including on shelves—at the LGM than today. This is greater than the frequently cited −125 m (e.g., 24, 80) that is usually based on observations uncorrected for isostatic effects. Heinrich event H2 at ∼19.5–22 ^{14}C ka (∼25 ka BP) (77, 81, 82) is not associated with a recognizable sea-level signal.

iii) Onset of deglaciation at ∼21–20 ka BP with a short-lived global sea-level rise of ∼10–15 m before 18 ka. The evidence comes from the Bonaparte Gulf (37, 38), has been identified elsewhere (83, 84), and is supported by isolated observations from five other locations (Bengal Bay, Cape St Francis (South Africa), offshore Sydney, Barbados, Maldives) which, although less precise than the principal data set, spread the rise over a longer time interval than originally suggested. Chronologically, this rise occurs substantially later than the H2 event.

iv) A short period of near-constant sea level from ∼18–16.5 ka BP. Support for this comes from observations from Barbados, the Sunda Shelf, Bonaparte Gulf, Mayotte, and Cape St Francis.

v) A major phase of deglaciation from ∼16.5–7 ka BP. The total esl change in this interval is ∼120 m, at an average rate of ∼12 m·ka^{-1}, corresponding to a reduction of grounded ice volume of ∼45 × 10^6 km^3). Within this interval, significant departures from the average occur.

vi) A rise of ∼25 m from ∼16.5–15 ka BP at the long-term average rate of ∼12 m·ka^{-1}. The data are from Sunda, Tahiti, the East China Sea, Mayotte, and Australia. Chronologically, the onset of this rise occurs at the time of the H1 event dated at 16.8 ka (85) or 16 ka (86). This period of rising sea level is followed by a short period (∼500–600 y) of near-constant sea level.

vii) A high rate of sea-level rise starting at ∼14.5 ka BP of ∼500 y duration. The onset occurs at the start of the Bølling–Allerød warm period. Its duration could be <500 y because of uncertainties in chronology, and the globally averaged rise in sea level of ∼20 m occurs at a rate of ∼40 mm·y^{-1} or greater. This pulse, MWP-1A, has been identified separately in the records of Barbados (24), Sunda (33), and Tahiti (28, 87). Spatial variation in its amplitude can be expected because of the planet's elastic and gravitational response to rapid unloading of ice in either or both of the two hemispheres (88) with, based on the ice–earth models used here, model-predicted values ranging from ∼14 m for Barbados to ∼20 m for Tahiti (*SI Appendix*, Fig. S4). This compares with observational values of ∼15–20 m (24, 28) for Barbados and 12–22 m for Tahiti (28). Observational uncertainties remain large, including differences in the timing of this event as recorded at the different localities, and it is not possible from this evidence to ascertain the relative importance of the contribution of the two hemispheres to MWP-1A.

viii) A period of sea-level rise from ∼14 to ∼12.5 ka BP of ∼20 m in 1,500 y. The rate of rise is near the long-term average. Data are relatively dense in this interval and come from well-distributed sites (Barbados, Tahiti, Sunda, Huon Peninsula, Australia and New Zealand, Indian Ocean, and the Yellow and East China seas).

ix) A period of a much reduced rate of rise from ∼12.5–11.5 ka BP. This short duration pause in the sea-level rise has been tenuously noted before in both composite (89) and individual (27) records. The chronology corresponds to the timing of the Younger Dryas stadial of the Northern Hemisphere when retreat of the Northern Hemisphere ice sheets ceased momentarily.

x) A period from ∼11.4–8.2 ka BP of near-uniform global rise. The average rate of rise during this 3.3 ka interval was ∼15 m·ka^{-1} with little convincing evidence of variations in this rate. A rapid rise, MWP-1B, has been reported at ∼11.3 ka but remains elusive (27) and is not seen in the composite record other than as a slightly higher rate of increase to ∼16.5 mm·y^{-1} for a 500-y period immediately after the Younger Dryas period.

xi) A reduced rate of sea-level rise for 8.2–6.7 ka BP. This is consistent with the final phase of North American deglaciation at ∼7 ka BP. A marked cooling event has been recorded at 8.2 ka BP in Greenland and North Atlantic cores (90), but there is no suggestion in the sea-level record of a corresponding fall or slowdown in global sea-level rise. The detailed local record from Singapore from 8.5 to 6 ka BP (40, 41) is consistent with the global rates within this interval except that a period of near-zero rise from 7.8 to 7.4 ka is not seen globally, possibly lost in the noise of other observations at around this time, possibly because it reflects local phenomena (Fig. 4).

xii) A progressive decrease in rate of rise from 6.7 ka to recent time. This interval comprises nearly 60% of the database (Fig. 1). The total global rise for the past 6.7 ka was ∼4 m (∼1.2 × 10^6 km^3 of grounded ice), of which ∼3 m occurred in the interval 6.7–4.2 ka BP with a further rise of ≤1 m up to the time of onset of recent sea-level rise ∼100–150 y ago (91, 92). In this interval of 4.2 ka to ∼0.15 ka, there is no evidence for oscillations in global-mean sea level of amplitudes exceeding 15–20 cm on time scales of ∼200 y (about equal to the accuracy of radiocarbon ages for this period, taking into consideration reservoir uncertainties; also, bins of 200 y contain an average of ∼15 observations/bin). This absence of oscillations in sea level for this period is consistent with the most complete record of microatoll data from Kiritimati (23). The record for the past 1,000 y is sparse compared with that from 1 to 6.7 ka BP, but there is no evidence in this data set to indicate that regional climate fluctuations, such as the Medieval warm period followed by the Little Ice Age, are associated with significant global sea-level oscillations.

ACKNOWLEDGMENTS. In addition to the support from our home institutions, this research has been partially funded by the Chaires Internationales de Recherche Blaise Pascal de l'État Français et la Région Île de France, the International Balzan Foundation, and the Australian Research Council. The development of the Baysian partition modeling software was partly supported by the Auscope Inversion Laboratory, funded by the Australian Federal Government.

1. Lambeck K, Chappell J (2001) Sea level change through the last glacial cycle. *Science* 292(5517):679–686.
2. Chappell J, Shackleton NJ (1986) Oxygen isotopes and sea level. *Nature* 324:137–140.
3. Waelbroeck C, et al. (2002) Sea-level and deep water temperature changes derived from benthic foraminifera isotopic records. *Quat Sci Rev* 21:295–305.
4. Ferranti L, et al. (2006) Markers of the last interglacial sea-level high stand along the coast of Italy: Tectonic implications. *Quat Int* 145-146:30–54.
5. Davies PJ, Marshall JF, Hopley D (1985) Relationships between reef growth and sea level in the Great Barrier Reef. *Proceedings of the Fifth International Coral Reef Congress* (Ecole Pratique des Hautes Etudes, Paris), Vol 5, pp 95–103.
6. Lambeck K, et al. (2011) Sea level and shoreline reconstructions for the Red Sea: Isostatic and tectonic considerations and implications for hominin migration out of Africa. *Quat Sci Rev* 30:3542–3574.
7. Shackleton NJ (1987) Oxygen isotopes, ice volume and sea level. *Quat Sci Rev* 6: 183–190.
8. Lisiecki LE, Raymo ME (2005) A Pliocene-Pleistocene stack of 57 globally distributed benthic δ^{18}O records. *Paleoceanography* 20(1):PA1003.
9. Shackleton NJ, Imbrie J, Hall MA (1983) Oxygen and carbon isotope record of East Pacific core V19-30: Implications for the formation of deep water in the late Pleistocene North Atlantic. *Earth Planet Sci Lett* 65:233–244.
10. Rohling EJ, et al. (2009) Antarctic temperature and global sea level closely coupled over the past five glacial cycles. *Nat Geosci* 2:500–504.
11. Moucha R, et al. (2008) Dynamic topography and long-term sea-level variations: There is no such thing as a stable continental platform. *Earth Planet Sci Lett* 271:101–108.
12. McKay NP, Overpeck JT, Otto-Bliesner BL (2011) The role of ocean thermal expansion in Last Interglacial sea level rise. *Geophys Res Lett* 38(14):L14605.
13. Cathles LM (1975) *The Viscosity of the Earth's Mantle* (Princeton Univ Press, Princeton, NJ).
14. Peltier WR, Andrews JT (1976) Glacial-isostatic adjustment-I. The forward problem. *Geophys J R Astron Soc* 46:605–646.
15. Nakada M, Lambeck K (1987) Glacial rebound and relative sea-level variations: A new appraisal. *Geophys J R Astron Soc* 90:171–224.
16. Mitrovica JX, Milne GA (2002) On the origin of late Holocene sea-level highstands within equatorial ocean basins. *Quat Sci Rev* 21:2179–2190.
17. Mitrovica JX, Wahr J (2011) Ice Age Earth rotation. *Annu Rev Earth Planet Sci* 39: 577–616.
18. Farrell WE, Clark JA (1976) On postglacial sea level. *Geophys J R Astron Soc* 46: 647–667.
19. Reimer PJ, et al. (2009) IntCal09 and Marine09 radiocarbon age calibration curves, 0–50,000 years cal BP. *Radiocarbon* 51:1111–1150.
20. Montaggioni LF (2009) *Quaternary Coral Reef Systems: History, Development Processes and Controlling Factors*, ed Braithwaite CJR (Elsevier, Amsterdam).
21. Woodroffe C, McLean R (1990) Microatolls and recent sea level change on coral atolls. *Nature* 344:531–534.
22. Chappell J (1983) Evidence for smoothly falling sea level relative to north Queensland, Australia, during the past 6,000 yr. *Nature* 302:406–408.

23. Woodroffe CD, McGregor HV, Lambeck K, Smithers SG, Fink D (2012) Mid-Pacific microatolls record sea-level stability over the past 5000 yr. *Geology* 40:951–954.
24. Fairbanks RG (1989) A 17,000-year glacio-eustatic sea level record: Influence of glacial melting rates on the Younger Dryas event and deep-ocean circulation. *Nature* 342: 637–642.
25. Bard E, Hamelin B, Fairbanks RG (1990) U-Th ages obtained by mass spectrometry in corals from Barbados: Sea level during the past 130,000 years. *Nature* 346:456–458.
26. Peltier WR, Fairbanks RG (2006) Global glacial ice volume and Last Glacial Maximum duration from an extended Barbados sea level record. *Quat Sci Rev* 25:3322–3337.
27. Bard E, Hamelin B, Delanghe-Sabatier D (2010) Deglacial meltwater pulse 1B and Younger Dryas sea levels revisited with boreholes at Tahiti. *Science* 327(5970): 1235–1237.
28. Deschamps P, et al. (2012) Ice-sheet collapse and sea-level rise at the Bølling warming 14,600 years ago. *Nature* 483(7391):559–564.
29. Chappell J, Polach H (1991) Post-glacial sea-level rise from a coral record at Huon Peninsula, Papua New Guinea. *Nature* 349:147–149.
30. Yokoyama Y, Esat TM, Lambeck K (2001) Coupled climate and sea-level changes deduced from Huon Peninsula coral terraces of the last ice age. *Earth Planet Sci Lett* 193:579–587.
31. Camoin GF, Montaggioni LF, Braithwaite CJR (2004) Late glacial to post glacial sea levels in the Western Indian Ocean. *Mar Geol* 206:119–146.
32. Van de Plassche O, ed. (1986) *Sea-Level Research: A Manual for the Collection and Evaluation of Data* (Geo Books, Norwich, UK).
33. Hanebuth T, Stattegger K, Grootes PM (2000) Rapid flooding of the Sunda Shelf: A late-glacial sea-level record. *Science* 288(5468):1033–1035.
34. Hanebuth TJJ, Stattegger K, Bojanowski A (2009) Termination of the Last Glacial Maximum sea-level lowstand: The Sunda-Shelf data revisited. *Global Planet Change* 66:76–84.
35. Zinke J, et al. (2003) Postglacial flooding history of Mayotte Lagoon (Comoro Archipelago, southwest Indian Ocean). *Mar Geol* 194:181–196.
36. Wiedicke M, Kudrass H-R, Hübscher C (1999) Oolitic beach barriers of the last Glacial sea-level lowstand at the outer Bengal shelf. *Mar Geol* 157:7–18.
37. Yokoyama Y, Lambeck K, Johnston P, Fifield LK, Fifield L, De Deckker P (2000) Timing of the Last Glacial Maximum from observed sea-level minima. *Nature* 406(6797): 713–716.
38. De Deckker P, Yokoyama Y (2009) Micropalaeontological evidence for Late Quaternary sea-level changes in Bonaparte Gulf, Australia. *Global Planet Change* 66:85–92.
39. Gibb JG (1986) A New Zealand regional Holocene eustatic sea level curve and its application for determination of vertical tectonic movements. *Bull R Soc N Z* 24: 377–395.
40. Bird MI, et al. (2007) An inflection in the rate of early mid-Holocene eustatic sea-level rise: A new sea-level curve from Singapore. *Estuarine Coastal Shelf Sci* 71:523–536.
41. Bird MI, et al. (2010) Punctuated eustatic sea-level rise in the early mid-Holocene. *Geology* 38:803–806.
42. Geyh MA, Kudrass H-R, Streif H (1979) Sea-level changes during the Late Pleistocene and Holocene in the Straits of Malacca. *Nature* 278:441–443.
43. Dutton A, Lambeck K (2012) Ice volume and sea level during the last interglacial. *Science* 337(6091):216–219.
44. Kopp RE, Simons FJ, Mitrovica JX, Maloof AC, Oppenheimer M (2013) A probabilistic assessment of sea level variations within the last interglacial stage. *Geophys J Int* 193: 711–716.
45. Xie X, Müller RD, Li S, Gong Z, Steinberger B (2006) Origin of anomalous subsidence along the northern South China Sea margin and its relationship to dynamic topography. *Mar Pet Geol* 23:745–765.
46. Lambeck K, Smither C, Johnston P (1998) Sea-level change, glacial rebound and mantle viscosity for northern Europe. *Geophys J Int* 134:102–144.
47. Paulson A, Zhong S, Wahr J (2007) Limitations on the inversion for mantle viscosity from postglacial rebound. *Geophys J Int* 168:1195–1209.
48. Peltier WR (1974) The impulse response of a Maxwell Earth. *Rev Geophys Space Phys* 12:649–669.
49. Mitrovica JX, Peltier WR (1992) A comparison of methods for the inversion of viscoelastic relaxation spectra. *Geophys J Int* 108:410–414.
50. Austermann J, Mitrovica JX, Latychev K, Milne A (2013) Barbados-based estimate of ice volume at Last Glacial Maximum affected by subducted plate. *Nat Geosci* 6:553–557.
51. Gallagher K, et al. (2011) Inference of abrupt changes in noisy geochemical records using transdimensional changepoint models. *Earth Planet Sci Lett* 311:182–194.
52. Milne GA, Mitrovica J (2008) Searching for eustasy in deglacial sea-level histories. *Quat Sci Rev* 27:2292–2302.
53. Nakada M, Lambeck K (1988) Late Pleistocene and Holocene sea-level: Implications for mantle rheology and the melting history of the Antarctic ice sheet. *J Seis Soc Jap* 41:443–455.
54. Nakada M, et al. (2000) Late Pleistocene and Holocene melting history of the Antarctic ice sheet derived from sea-level variations. *Mar Geol* 167:85–103.
55. Philippon G, et al. (2006) Evolution of the Antarctic ice sheet throughout the last deglaciation: A study with a new coupled climate—north and south hemisphere ice sheet model. *Earth Planet Sci Lett* 248:750–758.
56. Pollard D, DeConto RM (2009) Modelling West Antarctic ice sheet growth and collapse through the past five million years. *Nature* 458(7236):329–332.
57. Whitehouse PL, Bentley MJ, Le Brocq AM (2012) A deglacial model for Antarctica: Geological constraints and glaciological modelling as a basis for a new model of Antarctic glacial isostatic adjustment. *Quat Sci Rev* 32:1–24.
58. Anderson JB, Shipp SS, Lowe AL, Wellner JS, Mosola AB (2002) The Antarctic ice sheet during the Last Glacial Maximum and its subsequent retreat history: A review. *Quat Sci Rev* 21:49–70.
59. Cuffey K, Paterson WSB (2010) *The Physics of Glaciers* (Elsevier, Amsterdam).
60. Weidick A, Oerter H, Reeh N, Thomsen HH, Thorning L (1990) The recession of the inland ice margin during the Holocene climatic optimum in the Jakobshavn Isfjord area of West Greenland. *Global Planet Change* 2:389–399.
61. Briner JP, Håkansson L, Bennike O (2013) The deglaciation and neoglaciation of Upernavik Isstrøm, Greenland. *Quat Res* 80:459–467.
62. Stone JO, et al. (2003) Holocene deglaciation of Marie Byrd Land, West Antarctica. *Science* 299(5603):99–102.
63. Denton GH (1981) *The Last Great Ice Sheets*, ed Hughes TJ (Wiley, New York).
64. Lambeck K, Purcell A, Zhao J, Svensson N-O (2010) The Scandinavian Ice Sheet: From MIS 4 to the end of the Last Glacial Maximum. *Boreas* 39:410–435.
65. O'Connell RJ (1971) Pleistocene glaciation and the viscosity of the lower mantle. *Geophys J Int* 23:299–327.
66. Johnston P, Lambeck K (1999) Postglacial rebound and sea level contributions to changes in the geoid and the Earth's rotation axis. *Geophys J Int* 136:537–558.
67. Kaufmann G, Lambeck K (2002) Glacial isostatic adjustment and the radial viscosity profile from inverse modeling. *J Geophys Res* 107(B11):2280.
68. Hager BH, Richards MA (1989) Long-wavelength variations in Earth's geoid: Physical models and dynamical implications. *Philos Trans R Soc A Math Phys. Eng Sci* 328: 309–327.
69. Ricard Y, Wuming B (1991) Inferring the viscosity and the 3-D density structure of the mantle from geoid, topography and plate velocities. *Geophys J Int* 105:561–571.
70. King SD, Masters G (1992) An inversion for radial viscosity structure using seismic tomography. *Geophys Res Lett* 19:1551–1554.
71. Čadek O, Fleitout L (1999) A global geoid model with imposed plate velocities and partial layering. *J Geophys Res* 104(B12):29055–29075.
72. Mitrovica JX, Forte AM (2004) A new inference of mantle viscosity based upon joint inversion of convection and glacial isostatic adjustment data. *Earth Planet Sci Lett* 225:177–189.
73. Steinberger B, Calderwood AR (2006) Models of large-scale viscous flow in the Earth's mantle with constraints from mineral physics and surface observations. *Geophys J Int* 167:1461–1481.
74. Čížková H, van den Berg AP, Spakman W, Matyska C (2012) The viscosity of Earth's lower mantle inferred from sinking speed of subducted lithosphere. *Phys Earth Planet Inter* 200-201:56–62.
75. Mangerud J, Gyllencreutz R, Lohne Ø, Svendsen JI (2011) Glacial history of Norway. *Quaternary Glaciations - Extent and Chronology: A Closer Look*, eds Ehlers J, Gibbard PL, Hughes PD (Elsevier, Amsterdam), pp 279–298.
76. Bond GC, Lotti R (1995) Iceberg discharges into the North Atlantic on millennial time scales during the last glaciation. *Science* 267(5200):1005–1010.
77. Marcott SA, et al. (2011) Ice-shelf collapse from subsurface warming as a trigger for Heinrich events. *Proc Natl Acad Sci USA* 108(33):13415–13419.
78. Boulton GS, Dongelmans P, Punkari M, Broadgate M (2001) Palaeoglaciology of an ice sheet through a glacial cycle: The European ice sheet through the Weichselian. *Quat Sci Rev* 20:591–625.
79. Dyke AS, et al. (2002) The Laurentide and Innuitian ice sheets during the Last Glacial Maximum. *Quat Sci Rev* 21:9–31.
80. Siddall M, et al. (2003) Sea-level fluctuations during the last glacial cycle. *Nature* 423(6942):853–858.
81. Vidal L, et al. (1999) Link between the North and South Atlantic during the Heinrich events of the last glacial period. *Clim Dyn* 15:909–919.
82. Grousset F, Pujol C, Labeyrie L, Auffret G, Boelaert A (2000) Were the North Atlantic Heinrich events triggered by the behavior of the European ice sheets? *Geology* 28: 123–126.
83. Clark PU, McCabe AM, Mix AC, Weaver AJ (2004) Rapid rise of sea level 19,000 years ago and its global implications. *Science* 304(5674):1141–1144.
84. Carlson AE, Clark PU (2012) Ice sheet sources of sea level rise and freshwater discharge during the last deglaciation. *Rev Geophys* 50(4), RG4007.
85. Clark PU, et al. (2001) Freshwater forcing of abrupt climate change during the last glaciation. *Science* 293(5528):283–287.
86. Hemming SR (2004) Heinrich events: Massive late Pleistocene detritus layers of the North Atlantic and their global climate imprint. *Rev Geophys* 42(1):RG1005.
87. Bard E, et al. (1996) Deglacial sea-level record from Tahiti corals and the timing of global meltwater discharge. *Nature* 382:241–244.
88. Clark P, Mitrovica J, Milne G, Tamisiea M (2002) Sea-level fingerprinting as a direct test for the source of global meltwater pulse IA. *Science* 295:2438–2441.
89. Lambeck K, Yokoyama Y, Purcell A (2002) Into and out of the Last Glacial Maximum sea level change during oxygen isotope stages 3-2. *Quat Sci Rev* 21:343–360.
90. Alley RB, et al. (1997) Holocene climatic instability: A prominent, widespread event 8200 yr ago. *Geology* 25:483–486.
91. Lambeck K, Anzidei M, Antonioli F, Benini A, Esposito A (2004) Sea level in Roman time in the Central Mediterranean and implications for recent change. *Earth Planet Sci Lett* 224:563–575.
92. Kemp AC, et al. (2009) Timing and magnitude of recent accelerated sea-level rise (North Carolina, United States). *Geology* 37:1035–1038.